

Letter

Wireless Power Transfer under Wide Distance Variation Using Dual Impedance Frequency

Woochan Lee  and Dukju Ahn *

Department of Electrical Engineering, Incheon National University, Incheon 22012, Korea; wlee@inu.ac.kr

* Correspondence: adjj22@gmail.com; Tel.: +82-32-835-8767

Received: 22 November 2019; Accepted: 5 January 2020; Published: 7 January 2020



Abstract: A dual-impedance operation, where coil impedance is controlled by operating frequency selection, is proposed to maintain optimum reflected impedance across coupling variation. More specifically, this work focuses on how high coupling between coils presents excessively high reflected resistance to transmitter (Tx) inverters, degrading the efficiency and output power of the inverter. To overcome this problem, the proposed system is equipped with dual-impedance coil and selects high- or low-impedance coil based on the ability to operate both at 200 kHz and 6.78 MHz frequencies. The reactive impedances of 6.78 MHz coils are designed to be higher than that of 200 kHz coils. Since the reflected resistance is proportional to the coil impedances and coupling squared, at close distance with high coupling coefficient, 200 kHz coils with low coil impedances are activated to prevent an excessive rise in reflected resistance. On the other hand, at large distance spacing with low coupling coefficient, 6.78 MHz coils with high coil impedances are activated so that sufficient reflected resistance is obtained even under the small coupling. The proposed system's advantages are the high efficiency and the elimination of bulky mechanical relay switches. Measured efficiencies are 88.6–50% across 10 coupling variations.

Keywords: inductive power; dual impedance; dual band; reflected resistance; frequency splitting

1. Introduction

One of the major goals in wireless power transfer research today is to accommodate wide distance variations with high efficiency. It has been noted that the distance variation may cause frequency splitting if the transmitter (Tx) and receiver (Rx) coils are brought close together [1–3]. Either delivered voltage or power efficiency experiences a decrease when the system operates at the resonant frequency of Tx coil and Rx coil.

Several techniques have been proposed to solve the frequency splitting problem [4–8]. Works [4,5] propose using special geometry for the resonators. Other solutions include adaptive matching networks which require bulky and mechanically moving relay switches [6–9]. Work [10] proposes the use of a variable inductor at the receiver, this would require an additional buck converter, meaning that the receiver would have two buck converters

For a two-coil system, it has been found that frequency splitting degrades the delivered power whereas coil-to-coil efficiency is not degraded at the center frequency [3]. However, this discussion does not consider Tx inverter efficiency. It is discussed later in this paper that the inverter efficiency can also be degraded at short distance spacing. Therefore, the problems of short distance operation are low output power and the efficiency of Tx inverters.

From the circuit viewpoint, an excessively high reflected resistance is the reason of frequency splitting and consequent degradations. Specifically, the coupling between Tx and Rx coils is abstracted as a reflected resistance, and this hypothetical resistor behaves as the load resistance of a Class-D

Tx inverter. Since the efficiency and output power of an inverter depends on its load resistance, the reflected resistance should remain within the appropriate range.

To solve the aforementioned issues, this paper proposes the use of a dual-impedance mode where impedance control is done by operating frequency selection depending on magnetic coupling. One of the advantages is the high efficiency, given that high-impedance coils are designed for long-distance condition while low-impedance coils are optimized for short distance. Moreover, the conventional capacitor-switch matrix used for adaptive impedance matching is not necessary. Therefore, mechanical relay switches, which need complex driving blocks and are susceptible to mechanical damage, are not necessary.

2. Inverter Degradations at Strong Coupling

Figure 1a illustrates the circuit model of a basic wireless power transfer system. From the viewpoint of the transmitter, the coupling with the receiver can be represented by the reflected resistance, R_{refl} , in Figure 1b where:

$$R_{refl} = k^2 \omega L_{TX} \frac{\omega L_{RX}}{R_L + R_{P2}} \quad (1)$$

In other words, the current/voltage characteristic of Figure 1a with receiver and coupling is equivalent to the current/voltage of Figure 1b with the reflected resistance. It is important to recognize that the load resistor of Tx inverter is the reflected resistance.

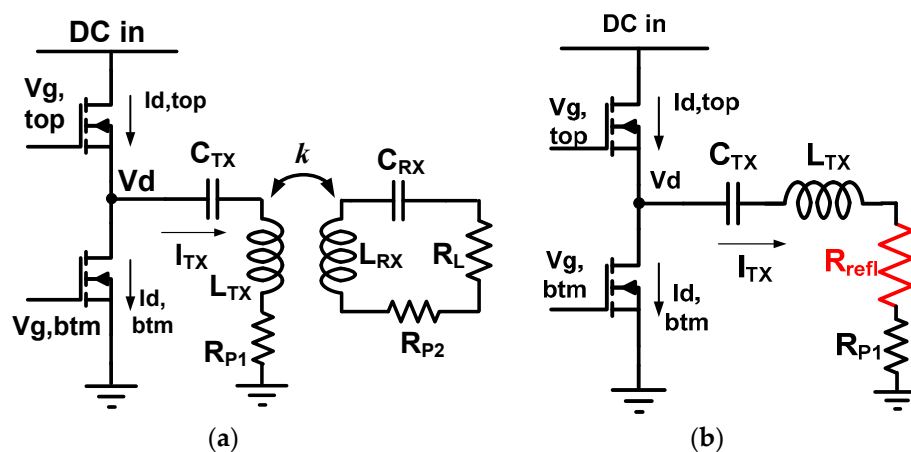


Figure 1. (a) Circuit model of a resonant wireless power transfer system. (b) From the viewpoint of the transmitter. The coupling with Rx is abstracted as reflected resistance, which serves as the load resistor of a Class-D inverter.

The normal zero-voltage switching (ZVS) waveform of inverter is shown in Figure 2a. After V_g , the upper limit is set to zero and both MOSFETs are off, the coil current (I_{TX}) discharges the parasitic drain capacitors of MOSFETs. This pulls down the drain voltage (V_d) to zero when both MOSFETs are off. After that, the bottom MOSFET is turned on with very low drain voltage (V_d). Therefore, switching loss is small in this case. The MOSFET used in this work is BUK9Y59-60E. Note that although $V_{g,btm}$ goes up at 123 ns, there is ~6 ns turn-on delay. Actual device turn-on point is approximately 128 ns.

However, this zero-voltage switching fails if the reflected resistance (R_{refl}) is too high [11]. High reflected resistance happens when the coupling between Tx and Rx is high at close distance as in Equation (1). This reduces I_{TX} as in Figure 2b. It then takes a longer time for the small I_{TX} to discharge the parasitic drain capacitance of MOSFETs. As a result, the V_d voltage cannot drop to zero before the turning-on of the bottom MOSFET as in Figure 2b, leading to switching loss [11–13].

Another problem of high reflected resistance is the significantly reduced output power of Tx inverters. As the load resistor of a Class-D inverter becomes larger, the output power of the inverter is reduced according to the function V_{DCin}^2 / R_{refl} [13].

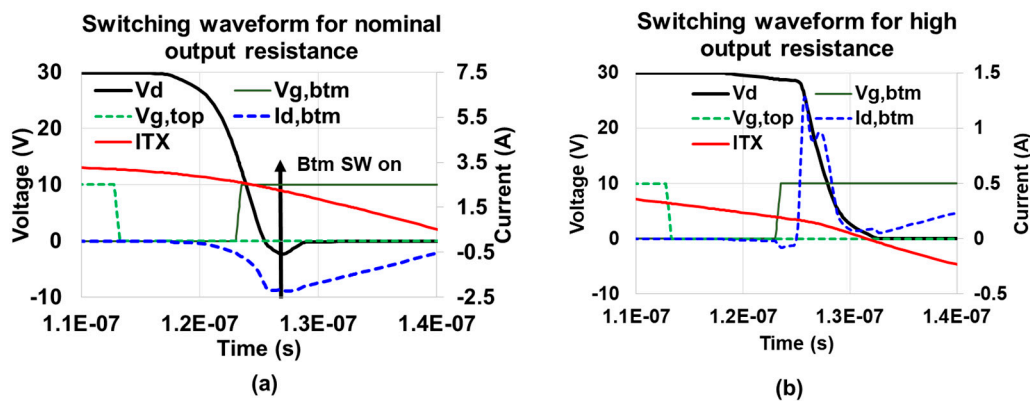


Figure 2. (a) Typical normal waveforms when the inverter is in zero-voltage switch mode. (b) When Tx and Rx are close together with high coupling. Zero-voltage switching fails due to excessive reflected resistance.

3. Proposed Dual-Impedance-Frequency Operation

The discussion in the previous section indicates that the reflected resistance should be maintained at the appropriate level. Therefore, this paper proposes dual-impedance operation by dual-frequency capability as in Figure 3a.

At a 200 kHz switching frequency, the current cannot flow toward $L_{T(R)XHI}$ because high-Z coils are tuned at ~ 6.78 MHz and behave as a large capacitive impedance at 200 kHz. Specifically, the impedance looking at a high-Z coil is $Z_{HI} = j\omega L_{HI} - j1/(\omega C_{6.78})$. At 6.78 MHz, the magnitude of ωL_{HI} and $1/(\omega C_{6.78})$ is comparable and thus they cancel each other out. However, for operation with low ω frequency (200 kHz), the ωL_{HI} term disappears whereas the $1/(\omega C_{6.78})$ term becomes enlarged. Hence, the total impedance becomes approximately $Z_{HI} = -j1/(\omega C_{6.78})$, which is capacitive. On the other hand, at a 6.78 MHz switching frequency, the currents cannot flow toward $L_{T(R)XLOW}$ because it behaves as large inductive impedance at 6.78 MHz switching frequency. The impedance looking at a low-Z branch which is tuned for 200 kHz is $Z_{LOW} = j\omega L_{LOW} - j1/(\omega C_{200})$. At 200 kHz, the magnitude of ωL and $1/(\omega C)$ are comparable and cancel each other. However, when ω becomes high (6.78 MHz), the $1/(\omega C_{200})$ term disappears whereas the ωL term becomes enlarged. Hence, the total impedance becomes approximately $Z_{LOW} = j\omega L_{LOW}$, which is inductive.

Therefore, the proposed coil enables dual-band operation without dedicated capacitor-selection switches. Changing the inverter driving frequency is enough for mode selection. The selected frequency bands are compatible with existing standard specification and frequency regulations. 200 kHz belongs to the Qi specification standards [14]. 6.78 MHz is the Industrial, Scientific and Medical (ISM) band which can be freely used [15], an example of which is AirFuel standards [16].

A method of adjusting coil impedance was proposed in [17]. However, this requires the coil to be split into many segments, and each segment should be connected to each relay switch. Another method of impedance reconfiguration is to use multiple capacitors and relay switches [9,18]. The drawback of these schemes is the use of relay switch. The solid-state relay in [17] can withstand only 0.2 W of power. Although mechanical relay switches can withstand higher power, its volume is too large, and its response time is slow. Moreover, a mechanical relay has a short lifetime and generates clicking sounds during operation. MOSFET or IGBT switches that are common in power electronics cannot be easily used to reconfigure resonant networks because the current at the resonant capacitor or coil is bi-directional. The intrinsic antiparallel diode within MOSFET or IGBT allows current flow from source (emitter) to drain (collector) terminal even if gate input is off. Two MOSFETs (IGBTs) should be connected in series with back-to-back configuration to block the bi-directional resonant current [19]. This increases the losses in switch and requires an additional isolated gate driver.

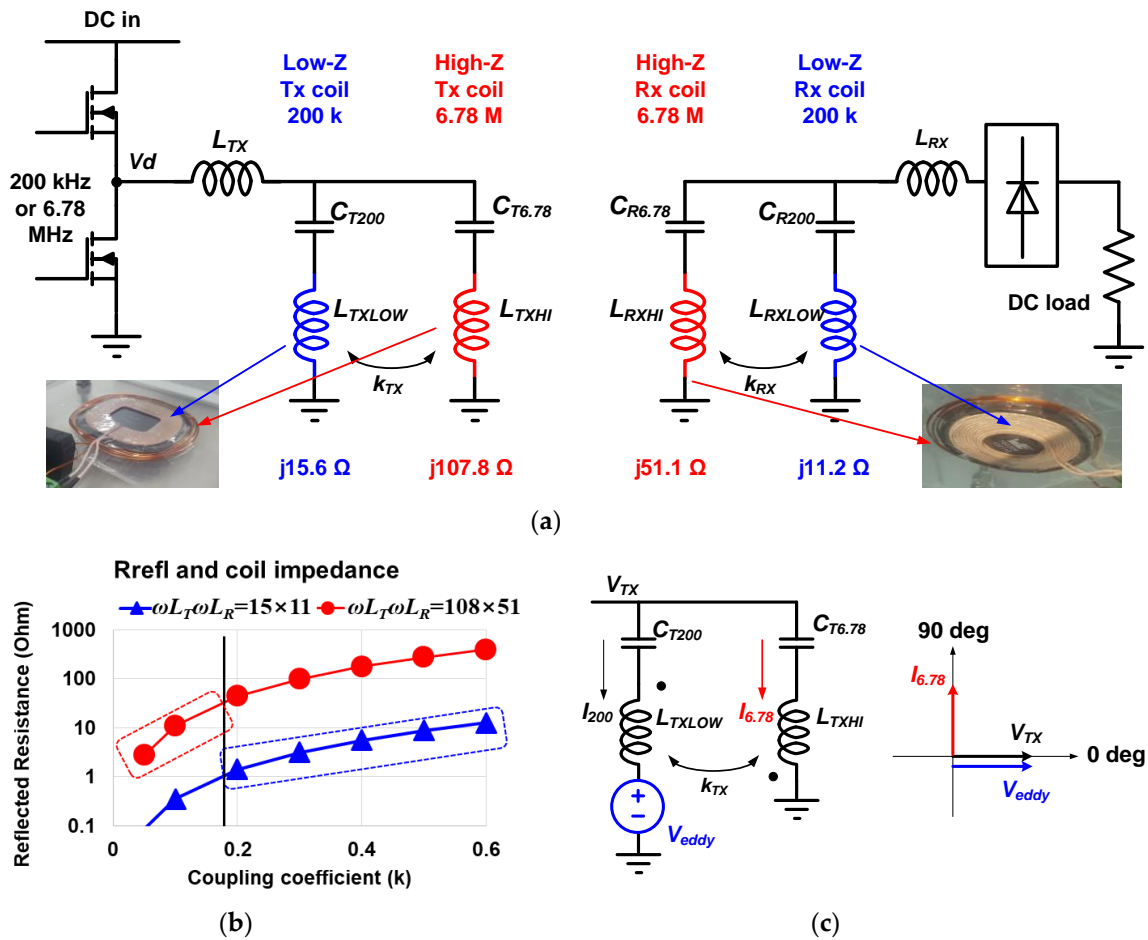


Figure 3. (a) Proposed dual-impedance operation by dual-frequency capability. For low-coupling condition, high-impedance coil paths are activated by 6.78 MHz operation. For high-coupling, low-impedance coil paths are activated. This can suppress excessive variations of reflected resistance which would serve as load resistor of Tx inverter, thus stabilizing the inverter efficiency. (b) The coil impedances are designed such that the reflected resistance is bounded within 1–30 Ω across the whole coupling coefficient k range. (c) Eddy current at $L_{T(R)XLOW}$ during 6.78 MHz mode is prevented by adjusting the magnitude and phase of $I_{6.78}$, so that V_{eddy} and V_{TX} are the same and the voltage across Low-Z path is zero [20].

The proposed method can handle high power without mechanical switches. Although two coils are used, the increment of volume is minimal because one coil is placed within the other coil concentrically.

The coil impedance is designed such that it is high at 6.78 MHz mode and low at 200 kHz. Hence, the coil impedance is adjusted by simply selecting the operating frequency. When the coupling k becomes low, the reflected resistance drops as in Equation (1). However, Equation (1) implies that the reflected resistance can be high if $\omega L_{TXHI} \omega L_{RXHI}$ is high even with the small coupling k . Therefore, the high-Z coils are activated by operating at 6.78 MHz. When the coupling k becomes too high, the reflected resistance becomes excessively high, resulting in the degradation of inverter efficiency as in Section 2. To prevent excessive rise of reflected resistance, small $\omega L_{TXLOW} \omega L_{RXLOW}$ is activated by 200 kHz switching frequency mode.

Referring to Figure 3b, the target range of reflected resistance, R_{refl} , is set to 1–30 Ω because, within this range, the inverter efficiency remains at least 84% or higher. This range of R_{refl} should be maintained across the whole operating distance of 0.5–4.4 cm, within which the coupling coefficient k varies from 0.057 to 0.6. For the blue triangular trace (low-Z coil) of Figure 3b, its reflected resistance drops below 1 Ω when the coupling k is lower than 0.17. At this low-coupling region, the red circular

trace (high-Z) can lift the reflected resistance to 30Ω . To this end, the high-Z coil is designed such that the multiplication of TX impedance and RX impedance of high-Z is 30 times higher than the multiplication of low-Z TX and RX impedances. The TX sector and the RX sector can have different impedance values—this does not affect the proposed design method. The RX is usually a movable device, and hence it is designed with smaller geometry and resultant lower impedance.

One practical issue is that, because $L_{T(R)XHI}$ and $L_{T(R)XLOW}$ are placed concentrically each other, high coupling between them exists, k_{TX} and k_{RX} . This coupling may cause an eddy current at $L_{T(R)XLOW}$ during 6.78 MHz switching frequency mode. To avoid this eddy current, $C_{T(R)6.78}$ is designed to be smaller than a value which would completely cancel the $L_{T(R)XHI}$ impedance [20]. Referring to Figure 3c, phasor diagram, the $I_{6.78}$ phase is faster than V_{TX} by 90 degree if $C_{T6.78}$ is chosen to be smaller than a value that resonates L_{TXHI} . From the dot convention and mutual inductance equation, the V_{eddy} is given as $V_{eddy} = -j\omega k_{TX} \sqrt{L_{TXHI}L_{TXLOW}}$, which becomes in-phase with V_{TX} . Therefore, the voltage difference across $L_{TXLOW}-C_{T200}$ is zero, which prevents eddy current. This allows closer placement of low-frequency coil and high-frequency coil each other than the coils of [21].

4. Measurement Result

Figure 4 shows measurement setup. The L_{TXHI} and L_{RXHI} are $2.53 \mu\text{H}$ and $1.2 \mu\text{H}$ and the L_{TXLOW} and L_{RXLOW} are $12.4 \mu\text{H}$ and $8.92 \mu\text{H}$, respectively. The C_{T200} and $C_{T6.78}$ are 55 nF and 130 pF , respectively. The C_{R200} and $C_{R6.78}$ are 64.1 nF and 252 pF , respectively.

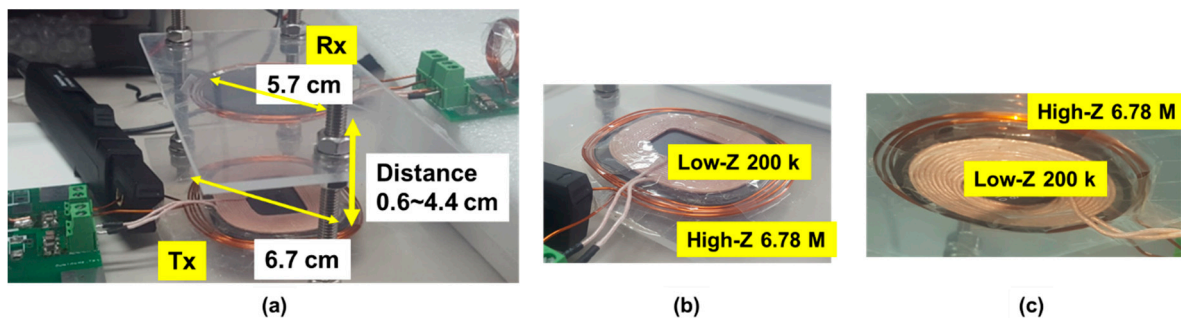


Figure 4. (a) Measurement setup. (b) Tx coils. Low-Z coils are within the high-Z coil. High-Z coil is wound around low-Z coil (c) Rx coils have similar configurations.

The distance between Tx and Rx varies from 0.6 cm to 4.4 cm. The corresponding coupling variation is from 0.6 to 0.057. The receiver output is 12 V–2 A, 24 W.

Figure 5 demonstrates the problems of excessively high reflected impedance. Figure 5a is the measured voltage and current waveform when the distance is only 1.1 cm and the reflected resistance is too high. The I_{TX} is suppressed due to high impedance, thereby causing longer delay for V_D to reach zero. The bottom MOSFET is turned on before V_D drops to zero, causing severe switching loss. On the other hand, the I_{TX} at 2.9 cm distance of Figure 5b is moderate and V_D can drop to zero before the bottom MOSFET is turned on. Zero-voltage switching is achieved in this case.

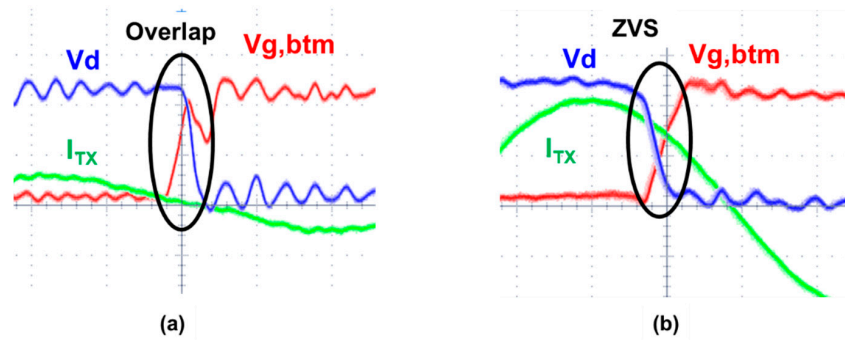


Figure 5. (a) Measured 6.78 MHz inverter waveforms at 1.1 cm distance (excessive reflected resistance). Gate is turned on before V_d drops to zero, causing switching losses. (b) 2.9 cm separation (moderate reflected resistance). Zero-voltage switching (ZVS) is achieved.

Figure 6a shows the measured efficiency and received voltage for the standalone single impedance system. The standalone single impedance system refers to the conventional single-frequency single-coil system. It is apparent that a single configuration cannot accommodate full distance range. Specifically, low-Z mode is better for 2 cm and below while high-Z performs better above 2 cm. The high-Z mode cannot output the required 12 V because of the excessive reflected resistance seen by the inverter.

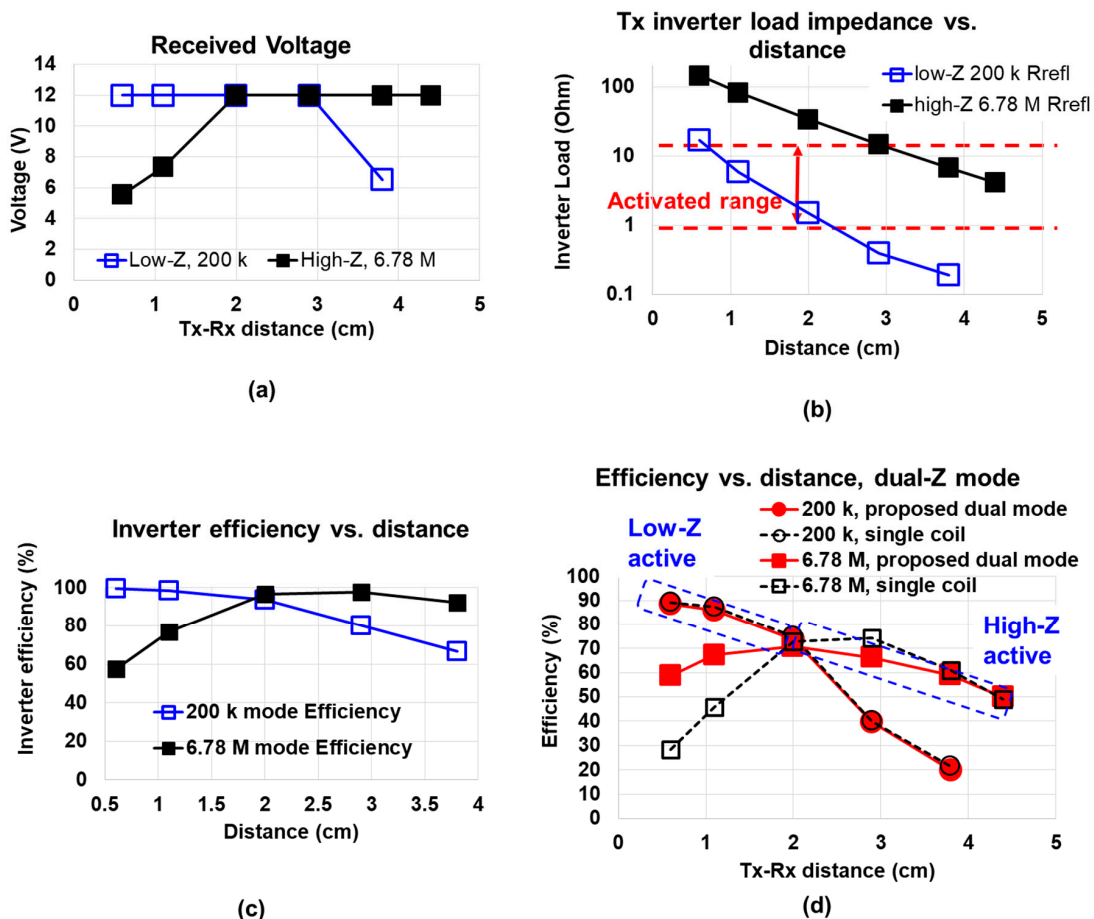


Figure 6. (a) Received voltage for conventional standalone single coil. A single configuration cannot accommodate the full distance range. (b) Measured reflected resistance for standalone low-Z and high-Z coils. (c) Simulated inverter efficiency. (d) Measured efficiency. The degradation from conventional single coil to proposed dual mode is minimal, which proves that Figure 3 successfully combines different standalone impedances into one dual-impedance system.

Figure 6b presents measured reflected resistance (i.e., inverter load) for standalone 200 kHz low-Z and 6.78 MHz high-Z configurations. At 1.1 cm and below, the inverter load resistor is too high. By introducing low-Z mode, the inverter load can be managed within $30\ \Omega$. Figure 6c shows inverter efficiencies. At 3–4 cm 200 k mode, the inverter load (reflected resistance) is too small, causing efficiency to drop. At 0.6–1.1 cm 6.78 MHz mode, inverter efficiency is degraded due to excessively high reflected resistance and ZVS failure. This is supported by Figure 5a,b.

In Figure 6d, it is proved that the two different standalone impedances are successfully merged into one dual-impedance system using Figure 3, because the efficiency degradation from standalone circuit to dual-impedance system is minimal. In a real usage scenario, the low-Z is activated simply by driving the Tx inverter to 200 kHz when reflected impedance becomes high, while the high-Z is activated by 6.78 MHz driving the inverter when reflected resistance becomes low.

One possible shortcoming of the proposed method is the parasitic resistance from L_{TX} and L_{RX} inductors. However, other matching techniques such as mechanical relays also cause parasitic resistance. Moreover, in Figure 6, at the longest distance (4.5 cm), the efficiency with the proposed method is the same as the efficiency of a single-mode coil. That means, the efficiency did not degrade due to the dual-mode capability.

5. Conclusions

A frequency-controlled dual-impedance operation which prevents excessive variation of inverter load is proposed. The low-impedance coils or the high-impedance coils are selected depending on coupling condition simply by frequency selection. This contrasts with the conventional impedance matching which relies on mechanical relay switch arrays to select capacitor bank or coil snippet.

The increment of coil volume is kept minimized by packing one coil within the other coil. The proposed method obviates the necessity of any impedance tuning switches—such as mechanical relays and back-to-back series semiconductor switches—which cause losses and high volumes. In summary, a compact, high efficiency, and mechanical-part-free method of impedance reconfiguration in response to coupling variation is realized.

Increasing the number of coils and frequency bands is not feasible at this moment because of the eddy current. For two coils in this paper, it is easy to prevent the eddy current following the scheme of Figure 3c. However, it is not directly applicable to more than 3 coils. Triple-band systems with eddy current blocking capability will be a topic for further research.

Author Contributions: Conceptualization, W.L.; Methodology, D.A.; Validation, D.A. and W.L.; Formal Analysis, W.L.; Investigation, W.L.; Resources, D.A.; Data Curation, D.A.; Writing—Original Draft Preparation, W.L.; Writing—Review & Editing, D.A.; Visualization, D.A.; Supervision, D.A.; Project Administration, D.A.; Funding Acquisition, D.A. All authors have read and agreed to the published version of the manuscript.

Funding: This work is supported by Incheon National University Grant (#2018-0482).

Conflicts of Interest: The authors declare no conflict of interest.

References

1. Liao, Z.-J.; Sun, Y.; Ye, Z.-H.; Tang, C.-S.; Wang, P.-Y. Resonant analysis of magnetic coupling wireless power transfer systems. *IEEE Trans. Power Electron.* **2019**, *33*, 5513–5523. [[CrossRef](#)]
2. Aditya, K.; Williamson, S. Design guidelines to avoid bifurcation in a series-series compensated inductive power transfer system. *IEEE Trans. Ind. Electron.* **2019**, *66*, 3973–3982. [[CrossRef](#)]
3. Ahn, D.; Hong, S. Effect of coupling between multiple transmitters or multiple receivers on wireless power transfer. *IEEE Trans. Ind. Electron.* **2013**, *60*, 2602–2613. [[CrossRef](#)]
4. Lee, W.-S.; Son, W.-I.; Oh, K.-S.; Yu, J.-W. Contactless energy transfer systems using antiparallel resonant loops. *IEEE Trans. Ind. Electron.* **2013**, *60*, 350–359. [[CrossRef](#)]
5. Lyu, Y.-L.; Meng, F.-Y.; Yang, G.-H.; Che, B.-J.; Wu, Q.; Sun, L.; Erni, D.; Li, J. A method of using nonidentical resonant coils for frequency splitting elimination in wireless power transfer. *IEEE Trans. Power Electron.* **2015**, *30*, 6097–6107. [[CrossRef](#)]

6. Lee, J.; Lim, Y.-S.; Yang, W.-J.; Lim, S.-O. Wireless power transfer system adaptive to change in coil separation. *IEEE Trans. Antennas Propagat* **2014**, *62*, 889–897. [[CrossRef](#)]
7. Kim, J.; Jeong, J. Range-adaptive wireless power transfer using multiloop and tunable matching techniques. *IEEE Trans. Ind. Electron.* **2015**, *62*, 6233–6241. [[CrossRef](#)]
8. Dang, Z.; Qahouq, J. Extended-Range Two-Coil Adaptively Reconfigurable Wireless Power Transfer System. In Proceedings of the IEEE Applied Power Electronics Conference and Exposition, Charlotte, NC, USA, 15–19 March 2015; pp. 1630–1636.
9. Jeong, S.; Lin, T.-H.; Tentzeris, M. A real-time range-adaptive impedance matching utilizing a machine learning strategy based on neural networks for wireless power transfer systems. *IEEE Trans. Microw. Theory Tech.* **2019**, *67*, 5340–5347. [[CrossRef](#)]
10. Mai, R.; Yue, P.; Liu, Y.; Zhang, Y.; He, Z. A dynamic tuning method utilizing inductor paralleled with load for inductive power transfer. *IEEE Trans. Power Electron.* **2018**, *33*, 10924–10934. [[CrossRef](#)]
11. Czarkowski, D.; Kazimierczuk, M. ZVS class D series resonant inverter—discrete-time state-space simulation and experimental results. *IEEE Trans. Circuits Syst. I* **1998**, *45*, 1141–1147. [[CrossRef](#)]
12. Erickson, R.W. Resonant Conversion. In *Fundamentals of Power Electronics*; Kluwer Academic Publishers: New York, NY, USA, 2001; pp. 723–726.
13. Grebennikov, A.; Sokal, N.O. *Switchmode RF Power Amplifiers*; Elsevier: Amsterdam, The Netherlands, 2007; pp. 78–79.
14. Wireless Power Consortium. *The Qi Wireless Power Transfer System Power Class 0 Specification*; Part 4: Reference designs, ver. 1.2.2, April. 2016; Wireless Power Consortium: Piscataway, NJ, USA, 2016.
15. International Telecommunication Union (ITU). *Wireless Power Transmission Using Technologies other than Radio Frequency Beam*; Report ITU-R SM.2303-1, 2015; International Telecommunication Union (ITU): Geneva, Switzerland, 2015.
16. AirFuel Alliance. Available online: <https://airfuel.org/> (accessed on 19 December 2019).
17. Mercier, P.; Chandrakasan, A. Rapid wireless capacitor charging using a multi-tapped inductively-coupled secondary coil. *IEEE Trans. Circuit Syst. I* **2013**, *60*, 2263–2272. [[CrossRef](#)]
18. Li, Y.; Hu, J.; Chen, F.; Liu, S.; Yan, Z.; He, Z. A new-variable-coil-structure-based IPT system with load-independent constant output current or voltage for charging electric bicycles. *IEEE Trans. Power Electron.* **2018**, *33*, 8226–8230. [[CrossRef](#)]
19. Erickson, R.W. Switch Realization. In *Fundamentals of Power Electronics*; Kluwer Academic Publishers: New York, NY, USA, 2001; p. 72.
20. Ahn, D.; Kim, S.; Kim, S.-W.; Moon, J.; Cho, I.-K. Wireless power transmitter and receiver supporting 200-kHz and 6.78-MHz dual-band operation without magnetic field canceling. *IEEE Trans. Power Electron.* **2017**, *32*, 7068–7082. [[CrossRef](#)]
21. Riehl, P.; Satyamoorthy, A.; Akram, H.; Yen, Y.-C.; Yang, J.-C.; Juan, B.; Lee, C.-M.; Lin, F.-C.; Muratov, V.; Plumb, W.; et al. Wireless power systems for mobile devices supporting inductive and resonant operating modes. *IEEE Trans. Microw. Theory Tech.* **2015**, *63*, 780–790. [[CrossRef](#)]

